Scattering of polarized and unpolarized nucleons from ^{28}Si

C. R. Howell, R. S. Pedroni,* G. M. Honoré,† K. Murphy,‡ R. C. Byrd,§ G. Tungate,** and R. L. Walter

Department of Physics, Duke University, Durham, North Carolina 27706
and Triangle Universities Nuclear Laboratory, Duke Station, Durham, North Carolina 27706

(Received 6 June 1988)

Measurements of the differential cross sections and analyzing powers have been made for ^{28}Si(n,n_0) and ^{28}Si(n,n_1) for incident neutron energies between 8 and 17 MeV. These data have been combined with previous differential and total cross-section data to obtain the most complete data set for neutron scattering from ^{28}Si over the 8–40 MeV energy range. The data have been described within the framework of a symmetric rotational model using phenomenological coupled-channels calculations. Nuclear moments were deduced and they are in good agreement with those obtained from electron scattering and Coulomb excitation measurements. Various calculations were performed to determine the sensitivity of the data and calculations to the signs of the potential deformation parameters β_2 and β_4. The systematic analysis of the analyzing power data enabled the determination of the deformation length for the spin-orbit potential. Comparisons between neutron- and proton-scattering data and calculations were made to test the sensitivity of this type of data to charge symmetry breaking in the nuclear force and to investigate the isospin dependence of the absorptive part of the nucleon-nucleus scattering potential for ^{28}Si. The results of these comparisons suggest that the differences between ^{28}Si$+n$ and ^{28}Si$+p$ scattering can be attributed solely to Coulomb effects.

I. INTRODUCTION

Nuclei in the $2s$-$1d$ shell are particularly interesting because of the highly collective nature of their low-lying excited states. One such nucleus which exemplifies the collective features of this family of nuclei is ^{28}Si. The large static quadrupole moments of ^{28}Si suggest that the low-lying states are associated with rotational modes of excitation. Within the scheme of the collective model of the nucleus, excitations of the low-lying states set the permanently deformed nucleus into rotation about some space fixed axis. The energy level spectrum provides additional evidence of the rotational nature of the excited states in ^{28}Si. Electron scattering provides precise measurements of the charge distribution and moments, and the study of electromagnetic interactions is generally a sensitive test of nuclear structure and the coupling constants involved in the collective excitations. Since hadronic probes are sensitive to the nuclear matter densities, knowledge obtained through elastic and inelastic scattering of nucleons supply necessary information for a complete description of the nuclear transition matrices.

The investigation of ^{28}Si using nucleons as a probe has progressed chronologically in the usual manner with the proton-scattering data and analyses preceding that of the neutron work. Analyses of ^{28}Si(p,p') data over the energy range from 14 to 40 MeV with coupled-channels (CC) calculations have yielded much information concerning the deformation parameters β_2 and β_4 of the central potential and the deformation parameter β_{so} of the spin-orbit potential.[1,2] Only recently have neutron-scattering data[3–5] of comparable accuracy to the proton data become available for this nucleus. With the exception of one of the analyses in Ref. 4, CC analyses of these high accuracy neutron data have been conducted only at single energies or over narrow energy ranges spanning 10 MeV at most. Consequently, conclusions about the energy dependencies of the neutron-nucleus interaction for this nucleus over broad energy ranges are quite limited. Even the analyses by Austin and his collaborators,[4] which spanned the energy range from 11 to 40 MeV, only included neutron differential cross sections at 4 or 5 energies, consequently leaving sizable energy gaps in their study. Although the analysis of Martin[5] included an impressive set of neutron-scattering data, it was conducted with a spherical optical model (SOM) which provided little or no information about the collective properties of the nuclear interaction.

The objectives of the present investigation are: (1) to study the collective properties of the low-lying states in ^{28}Si using neutrons as a probe; (2) to determine the energy dependences of the optical-model parameters for neutron scattering from ^{28}Si over a sizable energy range; (3) to parametrize for the first time the spin-orbit part of the optical-model potential for the ^{28}Si$+n$ scattering system; and (4) to extract differences in the real and imaginary parts of the optical-model potential derived by fitting neutron- and proton-scattering data for the purpose of testing for charge symmetry breaking (CSB) in the nuclear force and deducing information about the isospin dependence of the absorptive part of the optical-model potential for nucleon scattering from ^{28}Si. The fulfillment of these objectives required very accurate differential cross sections $\sigma(\theta)$, vector analyzing powers $A_y(\theta)$, and

neutron total cross sections σ_T over a relatively wide energy range. The neutron facilities at the Triangle Universities Nuclear Laboratory (TUNL) were used to fill the gaps in the existing $\sigma(\theta)$ data from 8 to 17 MeV and to provide a set of $A_y(\theta)$ data from 10 to 17 MeV. A preliminary report on the present work was given at the Burr Oak Conference in 1984.[6]

II. THE NEUTRON DATA SET

The present analysis, which was carried out over a wide energy range, utilized data from several references. High quality neutron-scattering data from recent measurements were collected and evaluated to form the most complete set of $\sigma(\theta)$ and $A_y(\theta)$ data for neutron scattering from ^{28}Si. At energies where several independent measurements existed, only the highest accuracy data were used.

The data set for $\sigma(\theta)$ spans an energy range from 8 to 40 MeV and consists of 24 angular distributions. Differential cross sections for elastic scattering and inelastic scattering to the first excited state at incident energies of 8.0, 10.0, 11.9, 14.0, and 16.9 MeV were measured at TUNL. Data for elastic and inelastic scattering at 9.8 and 14.8 MeV were obtained from G. Haouat *et al.*[3] of Bruyères-le-Châtel (BRC). The data at 11.0, 20.0, 21.7, and 26.0 MeV were measured at Ohio University (OHO) and were reported in Tailor's Ph.D. dissertation and in a recent paper by Alarçon and Rapaport.[3] The $\sigma(\theta)$ for elastic scattering at 30.3 and 40.0 MeV were measured at Michigan State University (MSU) by DeVito *et al.*[4] The relative uncertainties in the elastic distributions ranged from 2 to 5 % and those in the inelastic data were 5 to 10 %. All distributions had a 5% normalization uncertainty. Neutron total cross sections were taken from ENDF/B-5 for neutron energies below 20 MeV and from the data of Larson *et al.* at higher energies.[7]

All $A_y(\theta)$ data included in the data set were measured at TUNL using the pulsed-polarized beam facilities to be described in Sec. III B. The uncertainties in the $A_y(\theta)$ data ranged from 3 to 8 % for the elastic data and from 6 to 12 % for the inelastic distributions. There was a 2% normalization uncertainty in these data due to the uncertainty in the value of K_y^y, the polarization transfer coefficient for the ^{2}H($\vec{d}$,n)^{3}He reaction. The arrow indicates that the particle is polarized. Prior to these measurements only one $A_y(\theta)$ angular distribution for ^{28}Si+$\vec{n}$ had been reported above 8 MeV, that of Böttcher *et al.*[3] at 14.1 MeV. These latter data are discussed below.

At the time of our measurement of $A_y(\theta)$ at 14.0 MeV, we became aware of a concurrent experiment at Erlangen by Böttcher *et al.*[3] Since very little $A_y(\theta)$ data for neutron scattering exists for energies above 8 MeV, except for measurements from our lab, we welcomed a check on our data. Unfortunately, the methods were not completely independent, since the code JANE is used at both labs to correct the $A_y(\theta)$ data for multiple-scattered neutrons in the sample and for finite geometry effects. In their measurement, a dc beam, rather than a pulsed beam, was used and a proton-recoil spectrum stripping method was employed to unfold the yields for the elastic and inelastic scattering.

Figure 1 is a comparison of the present $A_y(\theta)$ data at 14.0 MeV to the Erlangen data at 14.1 MeV. With the exception of the differences in the $A_y(\theta)$ at 42° and near 115°, the two data sets for elastic scattering are consistent within about two standard deviations. The discrepancies around 42° and 100°–115° occur in regions where $\sigma(\theta)$ is relatively low. In such a situation it might be difficult to properly separate the yields for the individual neutron groups accurately using the techniques employed at Erlangen. Because of the inconsistences between the present data and the Erlangen data, the Erlangen data for elastic scattering are not included in the $A_y(\theta)$ data set for the present nuclear calculations. However, since the $A_y(\theta)$ in the angular region around 42° was very sensitive to the input parameters for the spin-orbit interaction in the nuclear model calculations, the Erlangen data point for elastic scattering at this angle was plotted along with the TUNL data for comparison to the calculations.

The $A_y(\theta)$ data for inelastic scattering are in fairer agreement except at angles beyond 135°. The similarity between the Erlangen inelastic scattering and elastic scattering data beyond 135° suggest that perhaps there

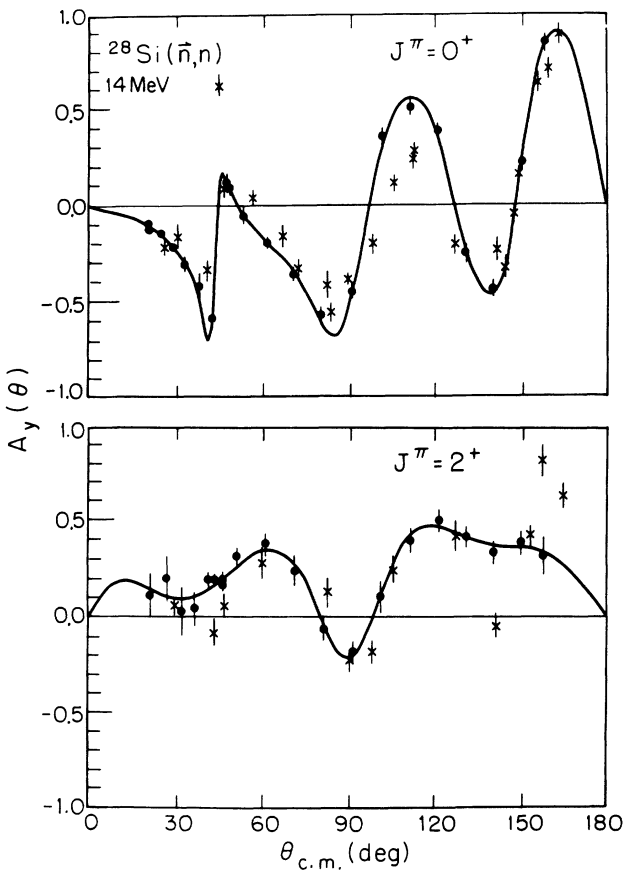

FIG. 1. A comparison of the present $A_y(\theta)$ data at 14 MeV to that of Böttcher *et al.*[3] The circles are the TUNL data and the crosses represent the Erlangen data. The curves are derived from associated Legendre polynomial fits to $A_y(\theta)\cdot\sigma(\theta)$ of the present data.

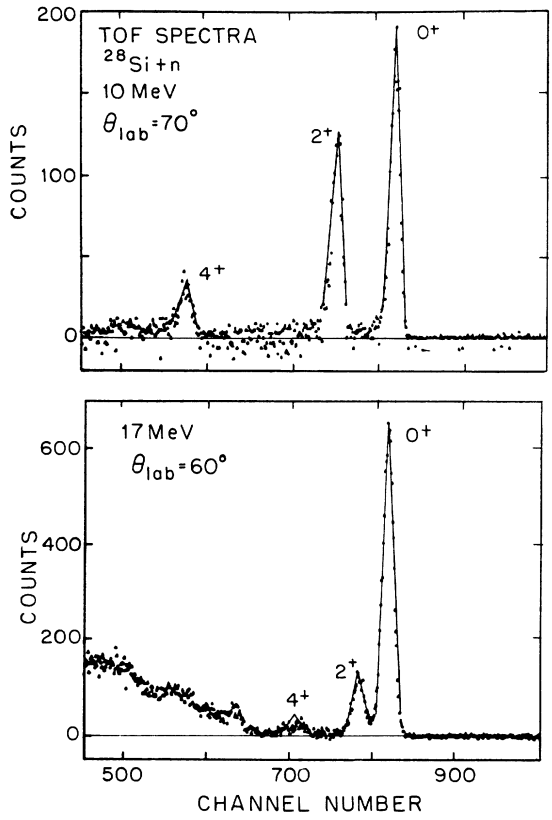

FIG. 2. TOF spectra at incident neutron enregies of 10 and 17 MeV. These spectra were obtained with a flight path of 6 m at $\theta=70°$ and $\theta=60°$, respectively.

was difficulty in resolving the elastic and inelastic yields using the Erlangen approach. In the time-of-flight (TOF) method employed at TUNL, the energy resolution of the experiment was more than adequate for resolving the elastically scattered neutrons from those that were inelastically scattered from the first excited state (see Fig. 2 and Ref. 8). Again, because of our concerns regarding the resolution problems in the Erlangen technique, only the TUNL data for inelastic scattering were used.

III. EXPERIMENTAL TECHNIQUES

Because detailed descriptions of the facilities at TUNL used to perform the neutron-scattering experiments have been reported previously,[8,9] only a brief discussion of techniques used in the present $\sigma(\theta)$ and $A_y(\theta)$ measurements will be presented here.

A. Experimental techniques for cross-section measurements

Differential cross sections for neutron scattering from natural silicon were measured at incident energies of 7.96, 9.95, 11.94, 13.97, and 16.92 MeV using the neutron TOF spectrometer at TUNL. A gas deuterium target was used to produce the neutrons via the ^{2}H$(d,n)^3$He source reaction. A deuterium pressure of 2 bar was maintained in a cylindrical cell about 0.8 cm in diameter and 3.16 cm long with its axis along the beam direction.

The deuteron beam employed in these measurements was accelerated by the tandem Van de Graaff at TUNL, which has a maximum terminal voltage of 8 MV. The beam was pulsed to permit the application of TOF techniques for determining the energy of the scattered neutrons. The neutrons emanating from the ^{2}H$(d,n)^3$He source reaction at angles around 0° were scattered from the silicon sample. The scattered neutrons were detected by two heavily shielded liquid scintillators which were positioned on opposite sides of the beam axis.

The scatterer was a cylinder with radius 1.18 cm and height 2.53 cm made of natural silicon, which is 92.6% ^{28}Si. The silicon sample was suspended directly over the pivot point of the two main detectors by a thin vertical steel cable, so that the axis of the cylindrical sample was perpendicular to the beam axis. The center-to-center distance from the neutron production target to the scatterer was typically 10 cm.

The neutron flux was monitored with a 5 cm (thick)$\times$5 cm (diameter) liquid scintillator which viewed the production target at a polar angle of 0° and an azimuthal angle of 50° above the scattering plane. Absolute normalization of the cross-section data was obtained by comparing to neutron scattering from hydrogen.

The backgrounds in the TOF spectra were small and found to be primarily due to sample-uncorrelated events in the neutron detectors. The sample-uncorrelated backgrounds were measured by accumulating TOF spectra with the sample removed. Very little background remained in the region of interest after the sample uncorrelated background was subtracted from the sample-in spectra, indicating that the sample-correlated backgrounds were negligible. Examples of the spectra with sample-uncorrelated backgrounds subtracted are shown in Fig. 2 for incident neutron energies of 10 and 17 MeV; these plots illustrate the energy resolution of the TOF spectrometer and the low sample-correlated backgrounds obtained with the system.

Corrections to the data for effects due to the finite sizes of the gas target, the silicon scatterer, and the neutron detectors were computed with the Monte Carlo code EFFIGY. The code EFFIGY was also used to correct the data for flux attenuation in the scatterer. The shift in the lab angle due to averaging over the angular acceptance of the scatterer and detector system was usually less than $\pm1°$ but was occasionally as high as $\pm2.5°$ on the steep forward-angle slope of the differential cross section for elastic scattering. The flux attenuation in the scatterer was generally less than 18%. The multiple-scattering corrections were less than 7% at most angles but were as high as 20% in the first minimum of the $\sigma(\theta)$ for elastic scattering.

The relative uncertainties include counting statistics and uncertainties in the Monte Carlo calculations. They varied from 3 to 10% for elastic scattering and from 3 to 20% for inelastic scattering. In addition, there exists a 5% overall normalization uncertainty for each angular distribution. However, the error bars associated with the data presented in this paper and used in the optical-model search procedures only reflect the relative uncertainties.

B. Experimental techniques for the analyzing power measurements

The analyzing power experiments were conducted in the same target room and used the same experimental arrangement as the cross-section measurements. These measurements were made at three incident neutron energies: 10.0, 14.0, and 17.0 MeV. The polarized neutrons were produced by the $^2\mathrm{H}(\vec{d},n)^3\mathrm{He}$ reaction initiated with polarized deuterons. Only the monoenergetic neutrons emitted near 0° were used. The incident polarized deuterons were produced with a Lamb-shift source. As in the $\sigma(\theta)$ measurements, the incident deuteron beam was pulsed to enable the use of TOF techniques for determining the energy of the scattered neutrons. This was achieved by using the highly efficient three-phase bunching system described in Ref. 10. The polarization of the deuteron beam was measured using the quench ratio method[11] and was typically about 70% on target. The standard beam intensity on target was 160 nA. Although this is a reasonable intensity for polarized beams, it is still over a factor of 10 smaller than the 2 μA of unpolarized beam used in the $\sigma(\theta)$ measurements. Therefore, to increase the counting rates in the $A_y(\theta)$ experiments, the deuterium gas pressure of the production target was increased from the 2 bar used in the $\sigma(\theta)$ measurements to 8 bar. Consequently, the energy spreads in the $A_y(\theta)$ measurements were normally around 460 keV full width at half maximum (FWHM), instead of the 140 keV in the $\sigma(\theta)$ measurements.

To minimize systematic errors the two neutron detectors were positioned symmetrically on opposite sides of the beam axis, thereby allowing a left-right asymmetry measurement at each angle. The spin quantization axis of the incident deuteron beam was flipped at the source, thus allowing a left-right asymmetry to be measured for spin-up and spin-down incident beams. The spin-up and spin-down left-right asymmetries were combined in the usual manner to minimize instrumental asymmetries.[12]

The Monte Carlo computer code JANE85 was used to correct the data for finite geometry effects, such as multiple scattering and flux attenuation in the sample. This code also determined the mean scattering angle due to the finite geometry of the entire experimental arrangement. The adjustments to the scattering angles were normally less than 1°. The multiple-scattering and flux-attenuation corrections were generally smaller than 5% of the measured $A_y(\theta)$ for elastic scattering and less than 2% for inelastic scattering. The corrections to the data for the angular resolution of the experiment were typically less than ± 0.02, except in the minima of the $\sigma(\theta)$ where they were as high as ± 0.12.

The relative uncertainties in the data are typically about ± 0.04 for the elastic scattering measurements and ± 0.07 for the inelastic scattering distributions. However, in the minima of the $\sigma(\theta)$ for elastic scattering the uncertainties are occasionally as high as ± 0.08. In addition to the relative uncertainties, there is an overall 3% normalization uncertainty due to the uncertainty in the value of $K_y^y(0°, E_d)$, the polarization transfer coefficient for the $^2\mathrm{H}(\vec{d},n)^3\mathrm{He}$ source reaction. The error bars shown on the data presented in this paper do not reflect this latter uncertainty, since it enters as a scale factor across each angular distribution.

IV. COMPOUND NUCLEUS CALCULATIONS FOR $^{28}\mathrm{Si}(n,n)$

Compound-nucleus (CN) calculations were performed using the computer code HAUSER*5, which was obtained from the nuclear analysis group at the Hanford Engineering Development Laboratory.[13] It has the capability of predicting total cross sections for bombarding energies up to 60 MeV. The code is based on three models of nuclear reactions: the statistical model (Hauser-Feshbach), the preequilibrium model, and the statistical model for direct reactions. We used the standard Hauser-Feshbach model for the present calculations.

The calculations included four particle channels (n, p, d, and α) plus the γ-ray channel. All level density parameters were taken from Gilbert and Cameron.[14] Although the (n,γ) cross section was negligible, it was included for completeness. Two-particle exit channels such as $(n,2n)$, (n,pn), and $(n,\alpha n)$ were neglected because of their large negative Q values and low cross sections at incident energies below 15 MeV, where CN contributions to scattering cross sections are most significant.

The particle transmission coefficients T_l were computed using optical-model parameters deduced from analyses of elastic scattering data for each residual nucleus. [The subscript l denotes the orbital angular momentum of the incident (exiting) particle relative to the target (residual) nucleus.] The coefficients for the neutron channel were computed with the CC code ECIS79 (Ref. 15) to explicitly account for the large inelastic scattering cross sections through coupling. All other T_l's were calculated with the code HAUSER*5, which used a SOM that did not include the spin-orbit interaction. The optical-model parameters used to compute the T_l's were taken from Refs. 16–18 and are listed in Table I. Plots of the T_l's for $l=0$, 2, and 4 are shown in Fig. 3. Only graphs for the first three even values of l are shown since the CN angular distributions $\sigma_{\alpha\beta}^{\mathrm{CN}}(\theta)$ are dominated by these angular momenta.

The CN calculations give good descriptions to the reaction cross sections, as shown in Fig. 4. Figure 4 is a plot of the $^{28}\mathrm{Si}(n,p)$ and $^{28}\mathrm{Si}(n,\alpha)$ cross sections for the sum of the ground state and lower three excited states in $^{28}\mathrm{Al}$ and $^{25}\mathrm{Mg}$, respectively. The data are from Refs. 19–21 and the curves are our predictions using the code HAUSER*5. The predicted total reaction cross sections are also in reasonably good agreement with the experimental data.

Width fluctuation corrections were applied to the CN calculations following the method of Gruppelaar and Reffo.[22] This type of correction accounts for effects due to correlations between the formation and decay channels in the compound nucleus system and was administered as a multiplicative factor $W_{\alpha\beta}$. The subscripts α and β denote the entrance and exit channels, respectively. Thus, all CN cross sections were modified as

$$\sigma_{\alpha\beta} \rightarrow \sigma_{\alpha\beta} W_{\alpha\beta} ,$$

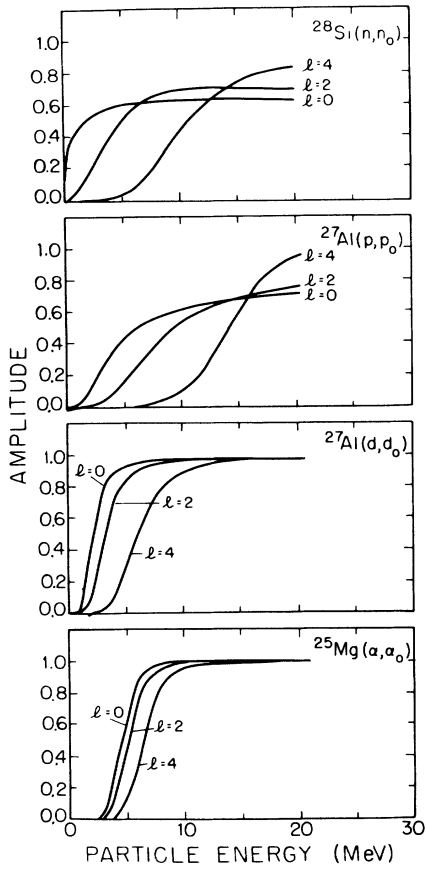

FIG. 3. Transmission coefficients T_l for particle exit channels in the $^{28}Si+n$ compound nucleus system.

where $W_{\alpha\beta}\sim 1+2\delta_{\alpha\beta}/\gamma_\beta$ and $\delta_{\alpha\beta}$ is the Kronicker delta function. Since the number of degrees of freedom γ_β is generaly about 2, the effect of $W_{\alpha\beta}$ is to enhance the elastic CN cross section by roughly a factor of 2 and to leave the the cross sections for the reaction channels essentially unchanged.

The CN cross sections were incoherently added to the results of our SOM and CC calculations. Figures 5 and 6 illustrate the influence of the CN contributions to the scattering cross sections at 10.0 and 14.8 MeV. The measured analyzing power was interpreted as the weighted average of an unpolarized constituent due to the CN formation and a polarized component due to the direct interaction between the incident neutron and the ^{28}Si nucleus:

$$A_y=\left[\frac{\sigma^{\mathrm{DI}}}{\sigma^{\mathrm{DI}}+\sigma^{\mathrm{CN}}}\right]A_y^{\mathrm{DI}}\ .$$

The differential cross section and analyzing power for the direct reaction, $\sigma^{\mathrm{DI}}(\theta)$ and $A_y^{DI}(\theta)$, were computed using either the SOM or CC computer code. The differential cross sections due to the CN formation $\sigma^{\mathrm{CN}}(\theta)$ for elastic scattering and inelastic scattering to the low-lying states in ^{28}Si were large at 10 MeV and decreased rapidly with increasing energy. In fact, at 14.8 MeV the CN contribu-

TABLE I. Optical-model parameters used in compound-nucleus calculations.

Reaction	V_{0R}[a] (MeV)	r_R (fm)	a_R (fm)	α_R[a]	W_{0D}[b] (MeV)	W_V[c] (MeV)	r_I (fm)	a_I (fm)	α_D[b]	α_V[c]	V_{so} (MeV)	r_{so} (fm)	a_{so} (fm)	References
$^{28}Si(n,n_0)$	53.9	1.17	0.62	−0.28	3.93	0.00	1.28	0.58	0.10	0.00	5.70	1.01	0.50	Preliminary[d]
$^{27}Al(p,p_0)$	55.9	1.25	0.65	−0.55	1.38	3.00	1.25	0.47	0.21	0.00	7.50	1.25	0.65	16
$^{27}Al(d,d_0)$	89.7	1.15	0.81	−0.22	14.40	0.00	1.34	0.68	0.00	0.00				17
$^{24}Mg(\alpha,\alpha_0)$	100.0	1.47	0.58	0.00	0.00	27.60	1.60	0.47	0.00	0.00				18

[a] $V_R=V_{0R}+\alpha_R E$.
[b] $W_D=W_{0D}+\alpha_D E$.
[c] $W_V=W_{0V}+\alpha_V E$.
[d] These parameters were taken from preliminary CC calculations; $\beta_2=-0.36$ and $\beta_4=0.20$ with $\delta_{so}=1.46\delta_C$.

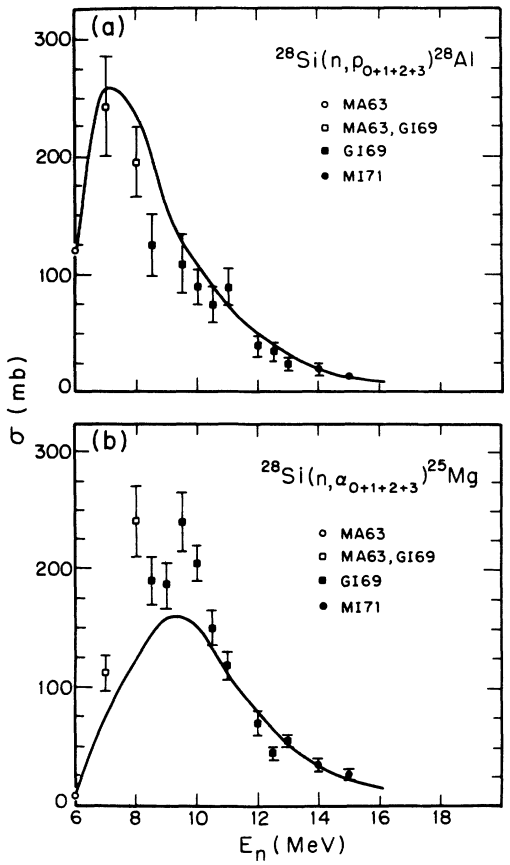

FIG. 4. Plots of the ^{28}Si(n,p) and ^{28}Si(n,α) partial cross sections. The open circles are from Ref. 19, solid squares from Ref. 20, solid circles from Ref. 21, and open squares are the average of data from Ref. 19 and 20. Curves are the present CN calculations.

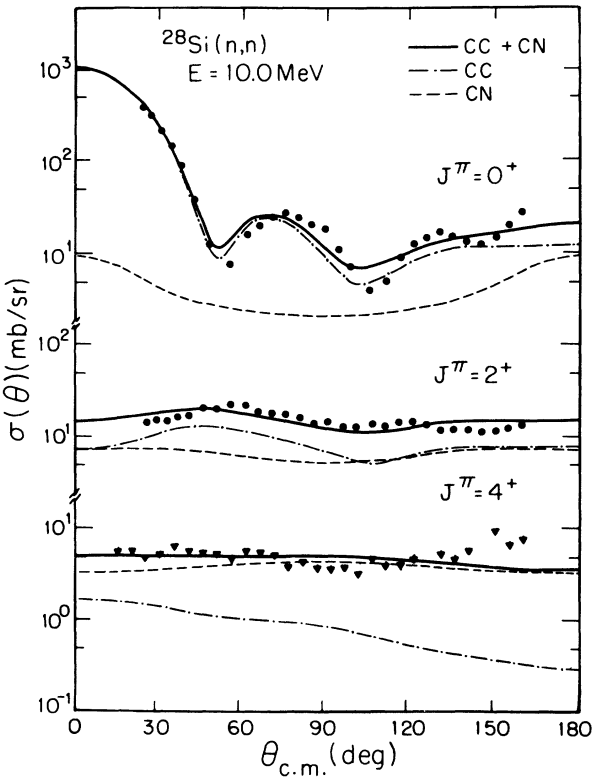

FIG. 5. Plots of $\sigma(\theta)$ at 10 MeV for elastic and inelastic neutron scattering. The dot-dashed curves represent the cross sections for the direct reaction computed with CC calculations, the dashed curves are due to CN contributions, and the solid curves are the sums of the direct reaction and CN contributions.

tions to the cross sections for scattering to the ground and 2^+ states were negligible as illustrated in Fig. 6. However, the CN contribution to the 4^+ cross section was still important at 14.8 MeV.

V. THE SPHERICAL OPTICAL-MODEL ANALYSIS OF ^{28}Si(n,n)

The SOM was an excellent tool for evaluating the current data set in an economical way. In addition, it provided the initial set of optical-model parameters for the more complicated and tedious CC calculations. In the SOM analysis a complex potential with Woods-Saxon form factors was used with the conventional form of the spin-orbit interaction. The central potential consisted of a real volume term, and surface and volume absorption terms. Sensitivity tests showed that the description of the $A_y(\theta)$ data did not require the inclusion of an imaginary spin-orbit term. The calculations were performed with a modified version of the search code GENOA obtained from F. Perey of the Oak Ridge National Laboratory. This modified version of the code included a correction term to approximately account for the Mott-Schwinger in-

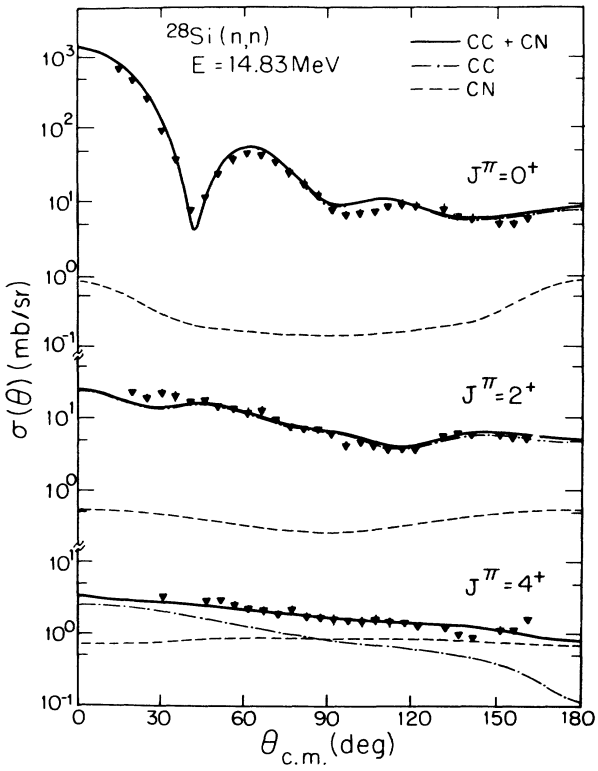

FIG. 6. Plots of $\sigma(\theta)$ at 14.83 MeV for elastic and inelastic neutron scattering. Curves are the same as in Fig. 5.

teraction.[23] Corrections for CN contributions were applied to both $\sigma(\theta)$ and $A_y(\theta)$ calculations at energies below 14 MeV, as described in Sec. IV.

The analysis was conducted in two steps. First, single-energy searches were done to obtain optimized parameters at each energy where data were available. The available $\sigma(\theta)$ and $A_y(\theta)$ distributions along with the σ_T data were simultaneously fitted. The starting parameters for each single-energy search were those of Böttcher *et al.*[3] In order to define the spin-orbit parameters early in the analysis, the energies at which both $\sigma(\theta)$ and $A_y(\theta)$ data were available were considered first. The potential strengths and geometry parameters of the real and imaginary potentials were simultaneously varied, and care was taken to avoid the notorious $V_R r_R$, $W_V r_I$, and $W_D a_I$ ambiguities. The optical-model parameters are defined as in Ref. 9. The rigorous constraints that $r_I \geq r_R \geq r_{so}$ and $a_R > a_I > a_{so}$, which were imposed by Van Oers *et al.*[24], were applied along with the requirement that all radius and diffuseness parameters be greater than 1.0 and 0.5 fm, respectively. The latter constraint was imposed because the $A_y(\theta)$ data consistently favored $r_{so} < 1.0$ fm and $a_{so} < 0.5$ fm, values which we felt were unphysical. The radius and diffuseness parameters of the volume imaginary potential were forced to be the same as those of the surface imaginary well. The single-energy fits are represented by the dashed curves in Figs. 7 and 8. The resulting geometry parameters were averaged for use in the next step.

The main goal in the second step was to obtain the en-

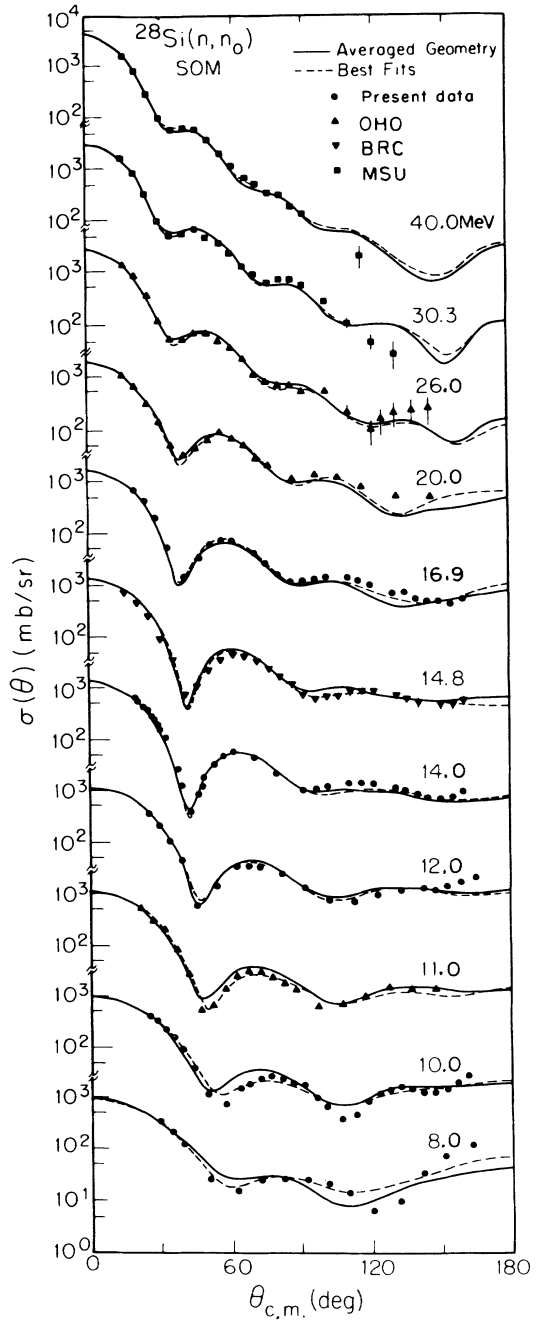

FIG. 7. SOM calculations compared to $\sigma(\theta)$ data for elastic scattering. The solid curves represent the fits with constant geometry and the dashed curves are resutls of the single-energy searches. All curves include CN contributions. Data include present measurements plus results from Ref. 3 and 4 as described in text.

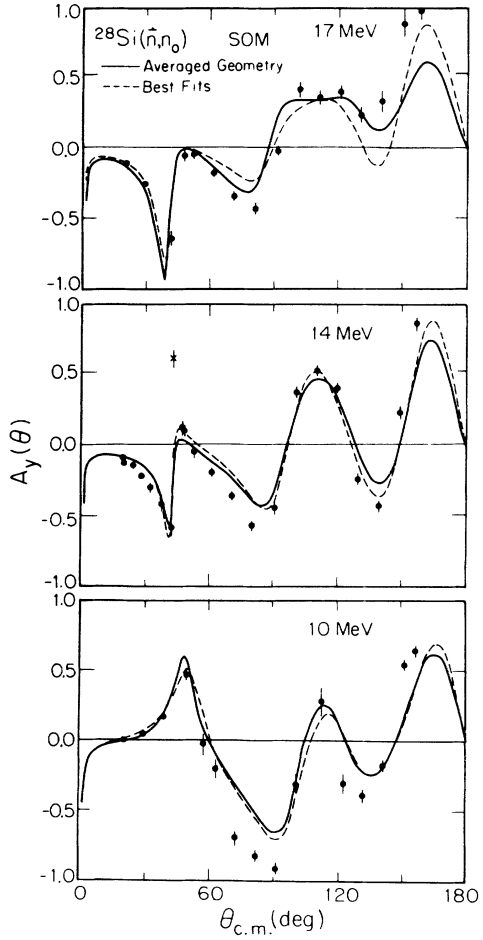

FIG. 8. SOM calculations compared to $A_y(\theta)$ data for elastic scattering. All curves are as explained in Fig. 7. The data are the present measurements plus one point at 14 MeV from the Erlangen experiment as described in the text.

ergy dependence of the strengths of the real potential V_R and the surface imaginary potential W_D. This was accomplished by searching only on V_R and W_D while holding the geometry parameters constant at the average values deduced above in step one. The energy-averaged geometry parameters were $r_R = 1.16$ fm, $a_R = 0.689$ fm, $r_I = 1.31$ fm, $a_I = 0.574$ fm, $r_{so} = 1.01$ fm, and $a_{so} = 0.500$ fm. The strength of the spin-orbit well V_{so} was also fixed to the average value determined in step one, which was $V_{so} = 6.60$ MeV. The volume absorption strength W_V could be suitably parametrized as

$$W_V = 0 \text{ MeV for } E \leq 13.3 \text{ MeV} ,$$

and

$$W_V = (-2.0 + 0.15E) \text{ MeV for } E > 13.3 \text{ MeV} .$$

The resulting fits are illustrated with the solid curves in Figs. 7 and 8. The resultant potential strengths and corresponding volume integrals per nucleon are plotted in Fig. 9. The potential strengths V_R and W_D could be described with simple linear energy dependences, as given in Fig. 9.

The success of the SOM suggest that there are no major problems with any of the data used in this analysis and that the parameters deduced should provide a good starting point for the CC calculations. Also, a good descritpion of the σ_T data was obtained over the energy range from 8 to 80 MeV using the linear energy dependences derived in the present analysis for neutron scattering data below 40 MeV. This agreement insures that the potential used in our model is a good representation of the mean nuclear field over the 8–80 MeV this energy range.

VI. COUPLED-CHANNELS ANALYSIS OF ^{28}Si(n,n)

The CC calculations used an optical potential and were performed with Raynal's search code ECIS79.[15] The 0^+, 2^+, and 4^+ states were modeled as the lower levels of a $K^\pi = 0^+$ rotational band. Starting with the average geometry parameters deduced in our SOM analysis, both geometry parameters and potential strengths were varied to optimize the fits to the elastic and inelastic data at each energy. As in the analysis using the SOM, the same geometry was used for the surface and volume imaginary potentials. Again, the $A_y(\theta)$ data preferred $r_{so} < 1.0$ fm and $a_{so} < 0.5$ fm. Consequently, we chose to fix these parameters to the values of $r_{so} = 1.01$ fm and $a_{so} = 0.5$ fm, which we set as the physically realistic lower limits on the radius and diffuseness parameters. After several iterations, a set of energy-averaged geometry and deformation parameters was derived. The resulting parameters were $r_R = 1.170$ fm, $a_R = 0.654$ fm, $r_I = 1.278$ fm, $a_I = 0.580$ fm, $r_{so} = 1.010$ fm, $a_{so} = 0.500$ fm, $\beta_2 = -0.38 \pm 0.01$, and

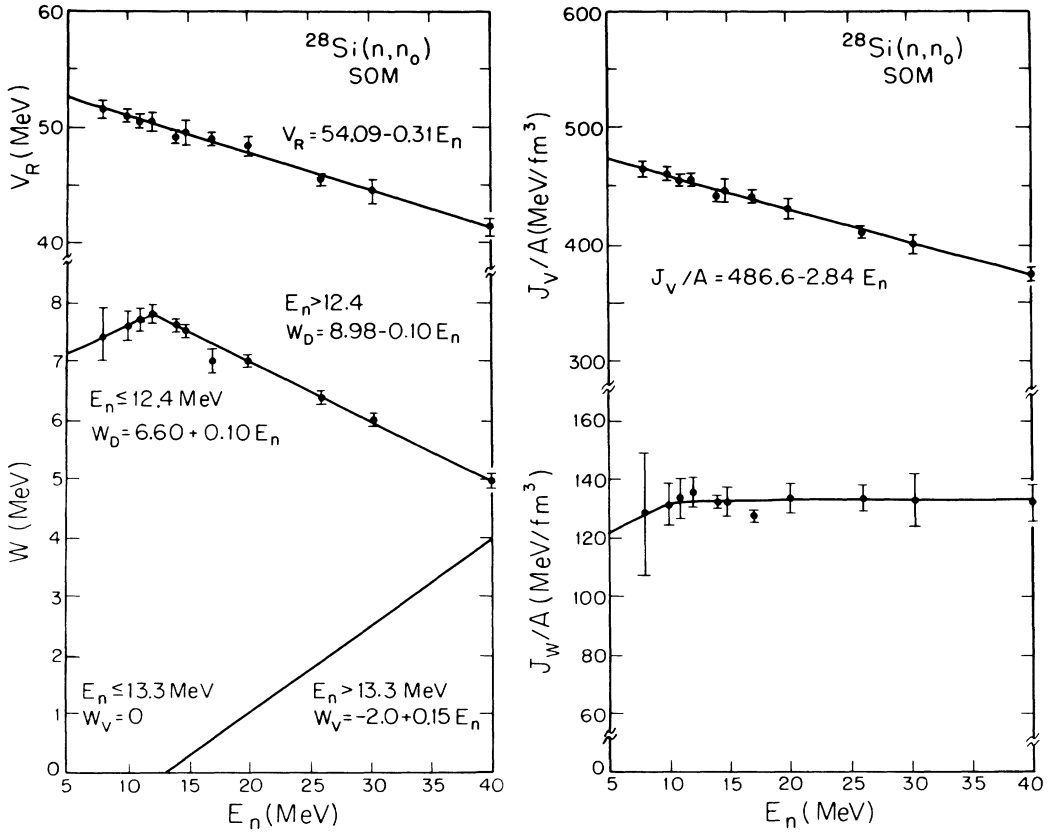

FIG. 9. Plots of the potential strengths and corresponding volume integrals per nucleon resulting from the present SOM analysis. The lines through the data points are least-square fits.

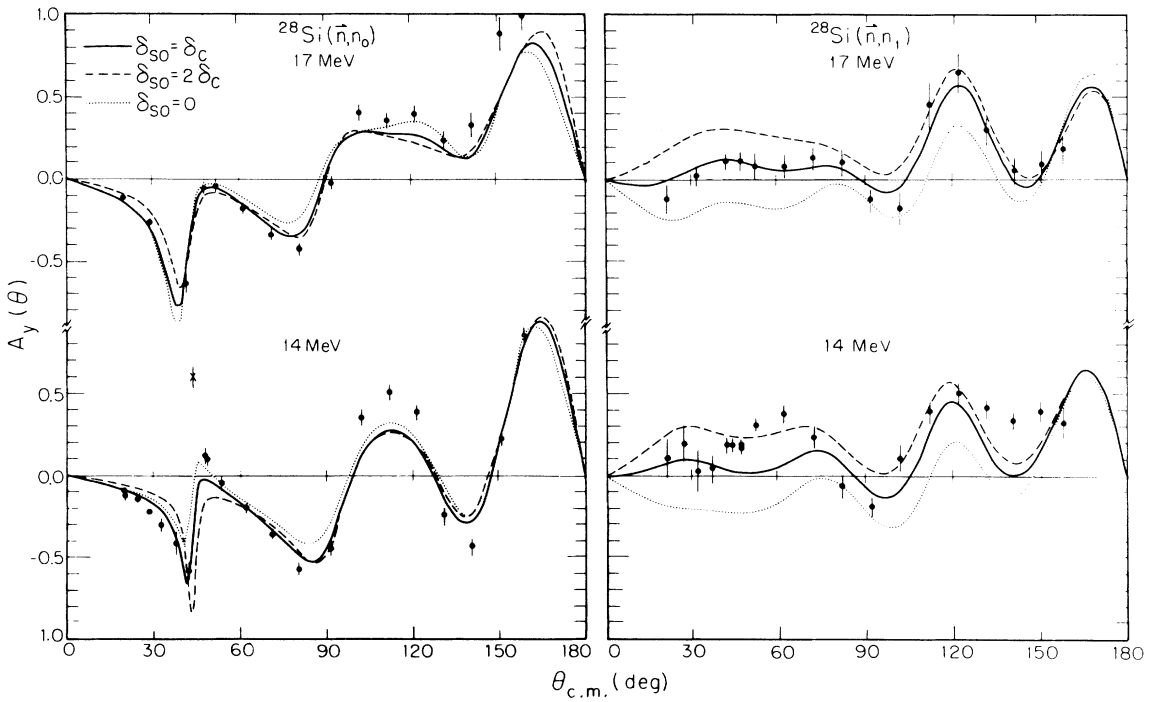

FIG. 10. CC calculations of $A_y(\theta)$ at 14 and 17 MeV for elastic scattering and inelastic scattering to the first 2^+ state. The solid curves represent calculations with $\delta_{so}=\delta_c$, the dashed curves are produced with $\delta_{so}=2\delta_c$, and the dotted curves correspond to $\delta_{so}=0$. The data are described in Fig. 8.

$\beta_4=+0.18\pm0.02$, where the parameters for the optical potential are defined as in Ref. 9, and β_2 and β_4 are the quadrupole and hexadecapole deformation parameters. The average strength of the spin-orbit potential was $V_{so}=6.0$ MeV. The deformation length of the spin-orbit potential $\delta_{so}=\beta_{so}R_{so}$ was varied to optimize the fits to the 2^+ $A_y(\theta)$ data. Figure 10 shows $A_y(\theta)$ data at 14 and 17 MeV in comparison with CC calculations using $\delta_{so}=0$, $\delta_{so}=\delta_c$, and $\delta_{so}=2\delta_c$, where δ_c is the deformation length of the central potential $\delta_c=\beta_c R_R$ with $R_R=r_R A^{1/3}$ and β_c representing either β_2 or β_4. The best value of δ_{so} was deduced to be $\delta_{so}=(1.2\pm0.2)\delta_c$.

New fits to the data were obtained using a constant geometry over the entire energy range from 8 to 40 MeV. The geometry parameters were fixed to the above values, and the volume absorption strength was held to the linear relationship derived in the SOM analysis. The deformation parameters and spin-orbit potential strength were also fixed to the above values. The fits were optimized at each energy by searching on V_R and W_D. The resulting calculations are illustrated with the solid curves in Figs. 11 and 12 and will be referred to as set A. The resultant values of V_R and W_D were parametrized with the simple linear energy dependences of

$$V_R=(53.61-0.29E)\text{ MeV},$$

and

$$W_D=(1.66+0.39E)\text{ MeV for } E\leq 11.0\text{ MeV},$$

and

$$W_D=(6.86-0.084E)\text{ MeV for } E>11.0\text{ MeV}.$$

Plots of the potential strengths and the parametrizing linear functions are shown in Fig. 13. The error bars on V_R and W_D represent the uncertainty in determining these parameters based on the accuracy of the data, the ability of the model to properly represent the data, and the correlation of these parameters to each other in the calculations. Calculations using the above smooth energy dependences are represented by the dashed curves in Figs. 11 and 12 and are denoted as set B.

The comparison of Figs. 7 and 8 for the SOM to Figs. 11 and 12 for the CC calculations shows that the two models describe the $\sigma(\theta)$ for elastic scattering equally well, except for the 8–11 MeV energy region where the CC model does notably better. Both models are about equally successful for describing the $A_y(\theta)$ data; each has some problems, but in different angular regions. We found that the CC searches quite closely preserved most of the parameters derived using the SOM. However, since neutrons which are removed from the elastic flux through inelastic scattering to the 2^+ and 4^+ states are explicitly accounted for in the CC model, W_D was smaller in the CC calculations than had been deduced using the SOM. More specifically, the values of W_D used in the CC calculations were about 20% smaller than the SOM values over the 10–40 MeV energy range.

Because the predictions of the analyzing power for neutron scattering from ^{28}Si have been shown by Böttcher *et al.*[3] to be very sensitive to the sign of β_2, we have performed calculations to test the sensitivity of the present data and model to the signs of β_2 and β_4. The $A_y(\theta)$ data at 10 MeV were not included in these tests because of the large CN contributions at this low energy.

In each case the geometry parameters and the value of V_{so} listed above were used, W_V was set to zero, and V_R and W_D were searched on to optimize the fits. Also, the magnitudes of β_2 and β_4 were fixed to their optimum values for 14 and 17 MeV. The results are shown in Figs. 14 and 15.

The fits to the data at 14 and 17 MeV preferred an oblate shaped potential ($\beta_2 < 0$) with $\beta_4 > 0$. The descriptions of the $\sigma(\theta)$ data for elastic scattering at back angles were very sensitive to the sign of β_2, with slightly better

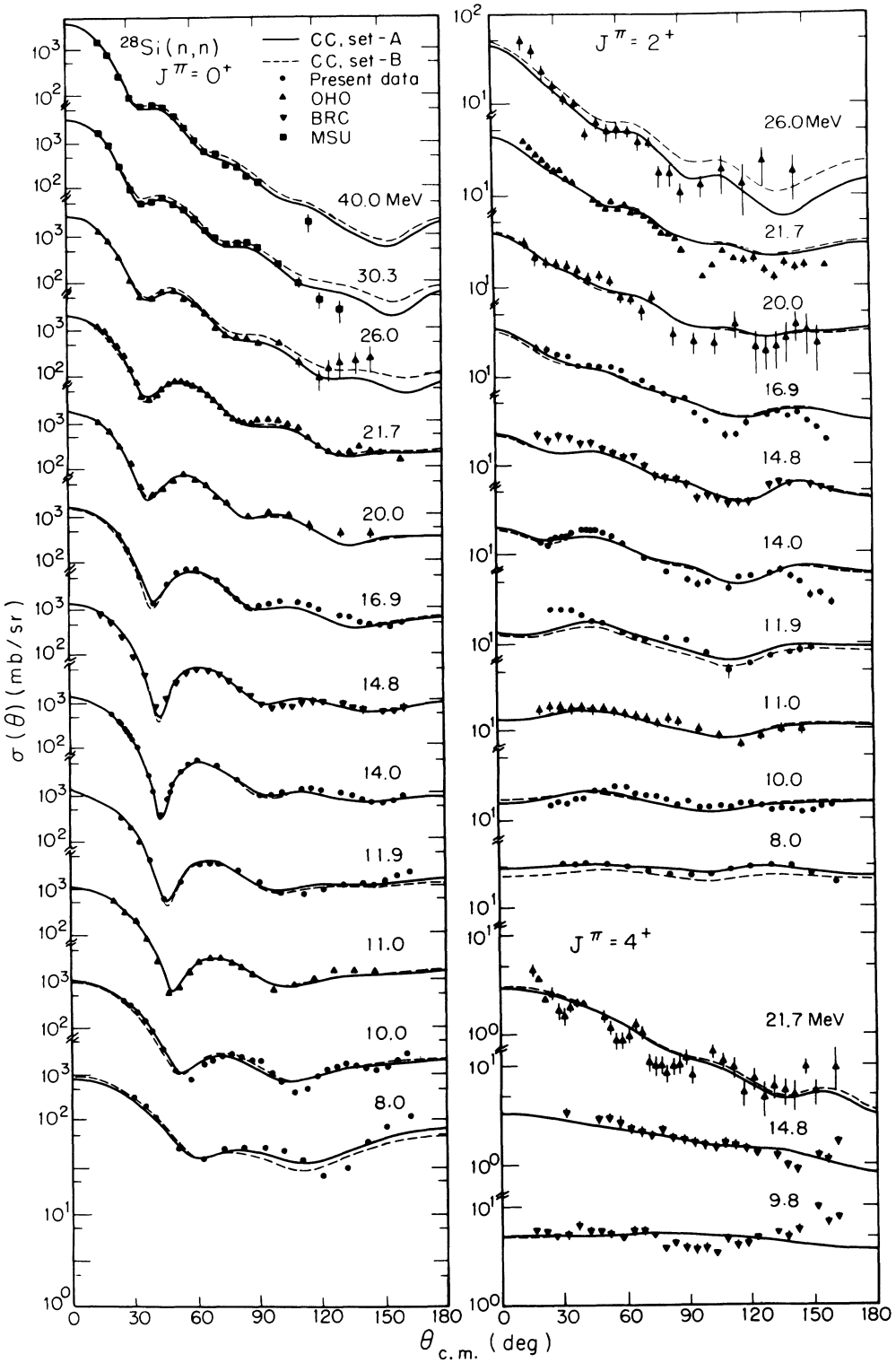

FIG. 11. The $\sigma(\theta)$ for elastic and inelastic scattering of neutrons. The curves are the results of CC calculations which model ^{28}Si as a symmetric rotor with the 0^+, 2^+, and 4^+ states forming the coupling basis. See text for a more detailed description of the curves. The data are the same as described in Fig. 7.

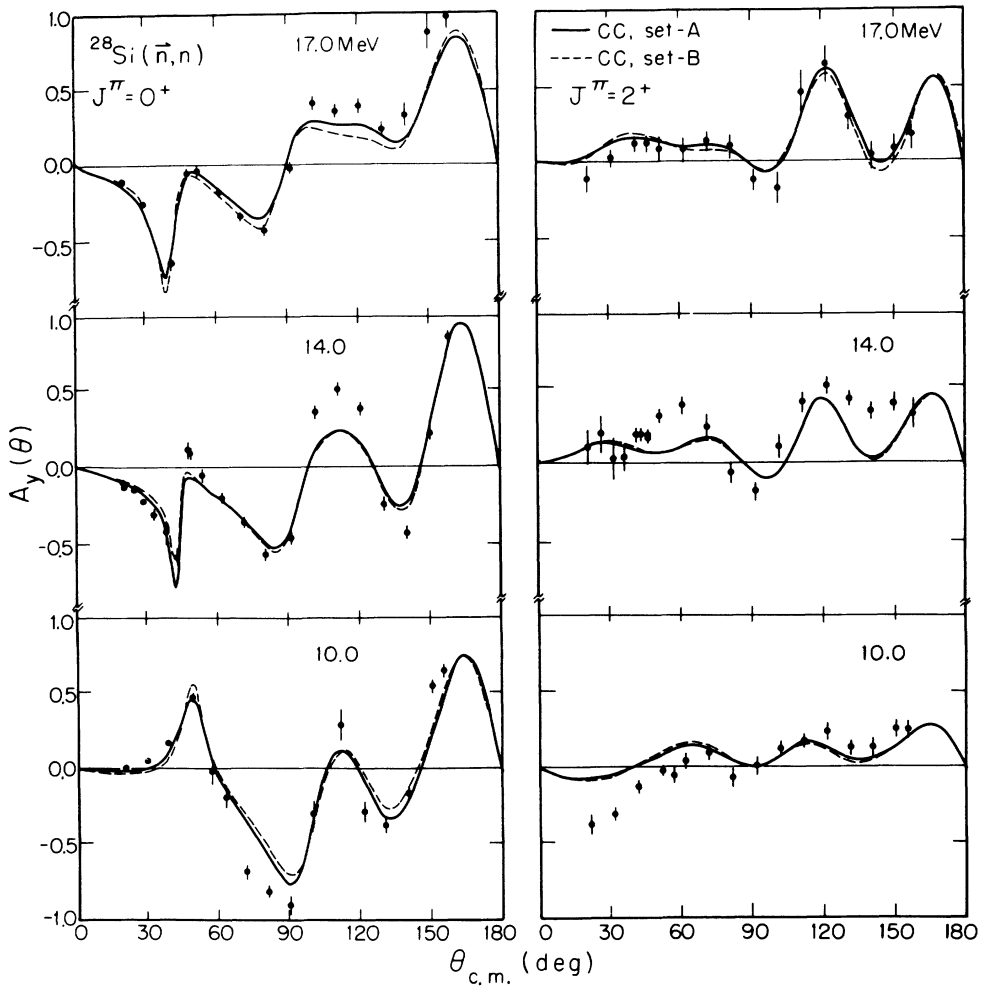

FIG. 12. The $A_y(\theta)$ for elastic and inelastic scattering of neutrons. The curves are the same as in Fig. 11. The data are the present measurements.

fits resulting for $\beta_2<0$. The quality of the fits to the $\sigma(\theta)$ data for inelastic scattering to the 2^+ state were about the same for both signs of β_2. However, this observable showed strong sensitivity to the sign of β_4. In particular, the calculations with $\beta_4<0$ fell substantially below the data. The calculations of $\sigma(\theta)$ for scattering to the 4^+ state showed little sensitivity to the signs of β_2 and β_4.

In general, most of the sensitivity to the signs of β_2 and β_4 in the calculation of the $A_y(\theta)$ for elastic scattering was in the backward angle region, $\theta_{c.m.}>110°$. However, at 14 MeV the calculated $A_y(\theta)$ for elastic scattering around $\theta_{c.m.}=42°$ was extremely sensitive to the sign of β_4. Böttcher *et al.*[3] cited a similar sensitivity to the values of the parameters for the spin-orbit potential, especially to a_{so}. In the present analysis, it was found that the $A_y(\theta)$ in this narrow angular region is also very sensitive to the parametrization of the real central potential. These findings suggest that the high sensitivity of $A_y(\theta)$ around $\theta_{c.m.}=42°$ to the optical-model parameters is due to some delicate interference and not an indication of an important physical phenomenon. That is, since $A_y(\theta)$ is inversely proportional to $\sigma(\theta)$, the combination of partial waves necessary to produce the very deep minimum in the elastic scattering $\sigma(\theta)$ around $\theta_{c.m.}=42°$ is also responsible for the strong sensitivity of $A_y(\theta)$ at this angle. Because of this delicate interference of partial waves in the angular region around the minimum of $\sigma(\theta)$, small changes in the optical-model parameters can produce drastic shape differences in $A_y(\theta)$ in this angular region. Therefore, the description of the $A_y(\theta)$ data in this narrow angular region should not be used as a test for determining the sign of β_4.

As expected, the data and calculations for back angle scattering showed a significantly higher sensitivity to the shape of the nuclear potential than did the forward angle scattering. In fact, the most sensitive observables to the signs of β_2 and β_4 were the back angle $A_y(\theta)$ for inelastic scattering to the 2^+ and 4^+ states, respectively. In all cases the data preferred $\beta_2<0$ and $\beta_4>0$. These findings were consistent with the accepted[25] signs of β_2 and β_4.

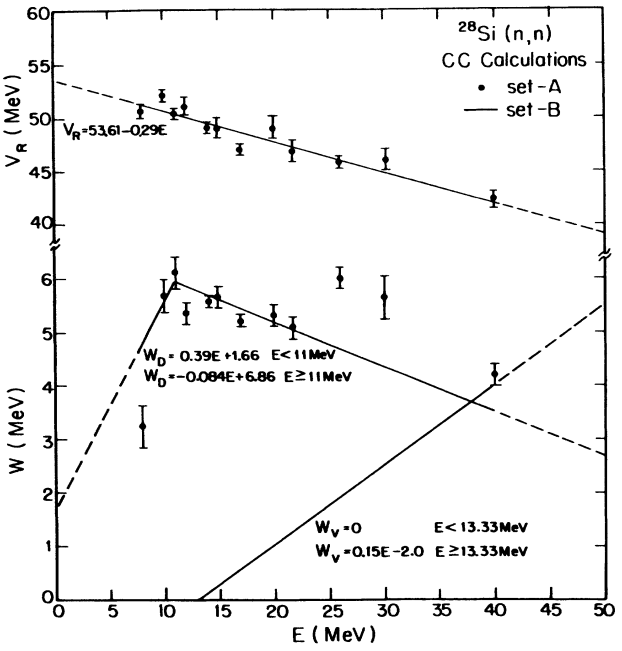

FIG. 13. Potential strengths of the real and imaginary wells versus incident neutron energy. The points are the results of single-energy searches on V_R and W_D. Parameter set B is a linear least-squares fit to the data points for each potential. The dashed extensions are extrapolations based on fitting neutron total cross sections.

VII. DETERMINATION OF MULTIPOLE MOMENTS FROM ^{28}Si(n,n') DATA

The normalized nuclear moments were calculated from our scattering potential as prescribed by Mackintosh.[26] The values of β_2 and β_4 deduced in Sec. VI give $Q_{20}=-1.49\pm0.05$ fm^2 and $Q_{40}=21.44\pm1.83$ fm^4 for the quadrupole and hexadecapole nuclear moments, respectively. These values are in excellent agreement with other hadron-scattering experiments.[1-3] Table II gives a comparison of the present results to multipole moments determined using inelastic electron scattering,[27,28] Coulomb excitation measurements,[29] Doppler-shift attenuation methods (DSAM),[30] and a deformed Hartree-Fock calculation with the Skyrme interaction (SII).[31] Only the magnitude of the moments are presented in Table II since the signs are not well determined in most measurements. The static moments $Q(2^+)$ and $Q(4^+)$ for the present analysis were taken as the product of N, the neutron number, times the normalized nuclear moments. The intrinsic moments Q_0 and H_0 were computed from the static moments as described by Bohr and Mottelson.[32] Multiplying the normalized moments by N instead of A permitted direct comparison to the electromagnetic (EM) results, since N and Z are equal for ^{28}Si.

Table II also illustrates the probe dependence in determining the transition probabilities. In the framework of the collective nuclear model, the transition probabilities are related to the intrinsic moments by

$$B(E2:\ 0^+\rightarrow 2^+)=\frac{5}{16\pi}\,|eQ_0|^2\,,$$

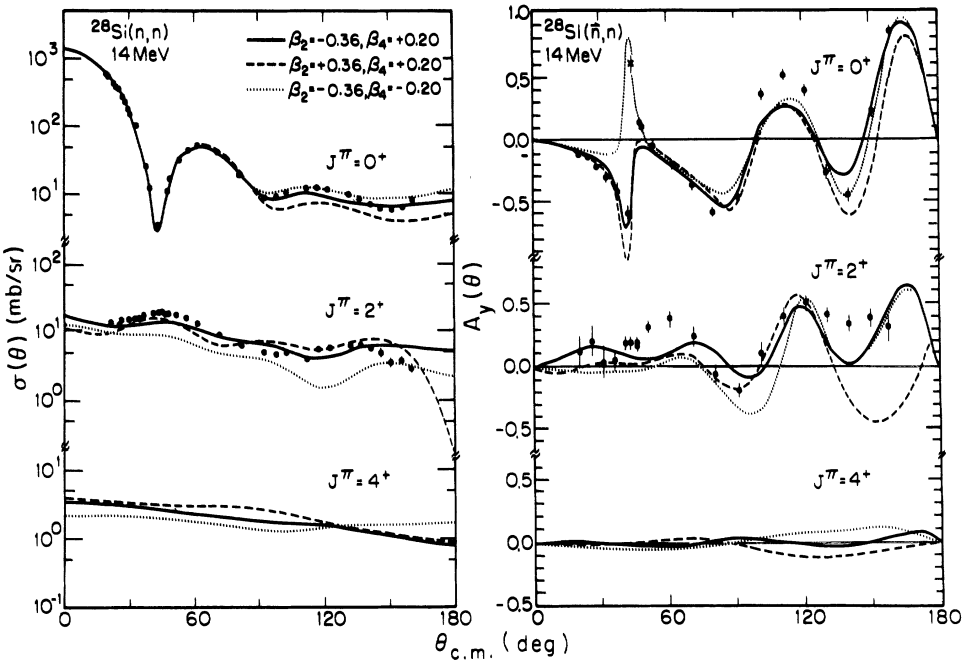

FIG. 14. CC calculations of $\sigma(\theta)$ and $A_y(\theta)$ at 14 MeV to illustrate the sensitivity of the data and calculations to the signs of β_2 and β_4. In all cases $\delta_{so}=1.2\delta_c$ and $W_V=0$, and V_R and W_D were searched on to optimize the fits.

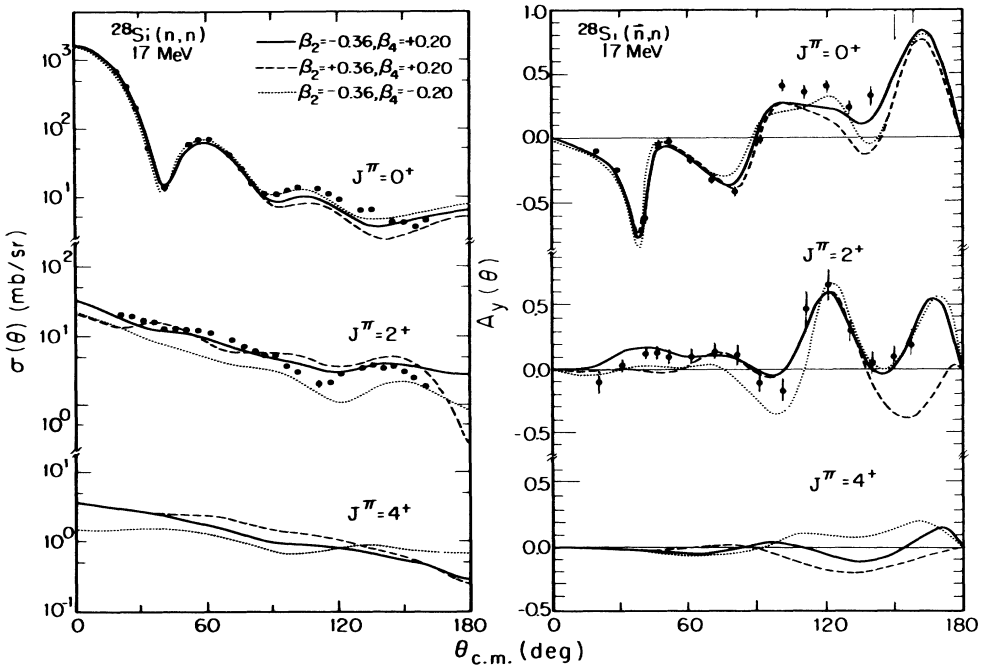

FIG. 15. Same as Fig. 14 except at an incident neutron energy of 17 MeV.

and

$$B(E4:\ 0^+\rightarrow 4^+)=\frac{9}{16\pi}\,|\,eH_0\,|^2\,.$$

More details are given in Refs. 31 and 32. The mean lifetime τ measured in Ref. 30 was converted to a $B(E2)$ value using the relationship given by Stelson and Grodzins.[33]

The intrinsic quadrupole moment and associated $B(E2)$ value deduced in the present work are 10–20% larger than those obtained using EM probes. There are two possible reasons for this discrepancy. First, according to Satchler's theorem[34] the normalized moments of the scattering potential are equal to the nuclear moments of the mass distribution only if the potential can be derived from a density independent folding potential. Perhaps the observed differences are an indication that the present optical potential can be obtained only with a density dependent nucleon-nucleon (N-N) interaction. Second, while hadronic probes interact via the strong force and therefore sample the entire nuclear matter distribution, EM probes couple only to the nuclear charge and current densities. Perhaps the observed discrepancies are due to small differences in the charge and mass distributions in the nucleus.

The present value of the intrinsic hexadecapole moment is about four times larger than the values obtained from (e,e') measurements and roughly 2.5 times larger than the Hartree-Fock calculations predict. Understandably, Q_{40} should be very sensitive to density dependent

TABLE II. Multipole moments and transition probabilities for ^{28}Si as a function of measurement technique. The $Q(2^+)$ and $Q(4^+)$ are the static quadrupole and hexadecapole moments, respectively. Q_0 and H_0 are the corresponding intrinsic moments.

	Multipole moments						
	Static		Intrinsic		Transition probabilities		
Measurement	$Q(2^+)$ (fm^2)	$Q(4^+)$ (fm^4)	Q_0 (fm^2)	H_0 (fm^4)	$[B(E2{:}0^+\rightarrow 2^+)]^{1/2}$ (e·fm^2)	$[B(E4{:}0^+\rightarrow 4^+)]^{1/2}$ (e·fm^4)	Ref.
(e,e')	18.3±0.9	74.5±12.0	64±3	205±33	20.2±0.9	86.7±14.0	27
	17.7±0.9	70.9±3.6	62±3	195±10	19.5±0.9	82.5±4.2	28
Coulomb ex. ^{208}Pb (^{28}Si, ^{28}Si)	17.5±2.4		61.3±8.4		18.7±0.5		29
DSAM (τ=0.677±0.035 ps)	16.3±0.4		57.2±1.5		18.1±0.5		30
HF calc. (SII) (charge moments)	17.1	113	60	310	18.9	130	31
(n,n)	20.9±0.7	300±26	73.0±2.5	826±70	23.0±0.8	349±30	Present

effects, departures from collective nuclear motion, and small differences in the charge and matter distributions. Also, it has been observed that the value for Q_{40} determined from hadron scattering data can vary considerably between analyses using the same probe.[26] Furthermore, it is not uncommon for the values of Q_{40} determined using hadronic probes to be larger by factors of 2–4 than those deduced from (e,e') scattering and EM data.[26,27] Perhaps a better determination of β_4 will bring the hadron-scattering results in closer agreement with (e,e') measurements. This could be achieved by making high quality measurements of angular distributions for neutron scattering to the 4^+ state. Such measurements are essential at energies above 20 MeV, where CN contributions are small.

VIII. COMPARISONS OF THE ANALYSES FOR ^{28}Si(n,n) AND ^{28}Si(p,p)

A. Coulomb correction to the real central potential

A direct comparison between analyses of neutron- and proton-scattering data gives the generic "Coulomb correction" terms to the optical potential. In addition to simply accounting for the slowing down of the incident protons by the Coulomb repulsion of the nucleus, these correction terms also include effects from all isospin dependent reaction mechanisms and forces. Although such comparisons do not provide information about specific aspects of the isospin differences between neutron and proton scattering, they are a useful guide for predicting proton-nucleus potentials from the corresponding Coulomb-free neutron-nucleus potentials.

For $T=0$ nuclei the real part of the central potential may be written as the sum of a neutron-nucleus potential plus a Coulomb correction term:

$$V(r,E)=V_n(r,E)+\Delta V_c(r,E) .$$

If $V_n(r,E)$ and $\Delta V_c(r,E)$ have the same radial dependence, which is normally taken to be the Woods-Saxon volume form, then only the relative strengths need to be considered:

$$V(E)=V_n(E)+\Delta V_c(E) .$$

Assuming a linear energy dependence for $V_n(E)$ will permit $\Delta V_c(E)$ to be essentially energy independent.[35] Thus, the strengths of the nuclear potential for neutron and proton scattering can be expressed as

$$V_n(E)=V_0-\alpha E ,$$

and

$$V_p(E)=V_0-\alpha E+\Delta V_c=V_n(E)+\Delta V_c .$$

Of course, this is assuming that the neutron- and proton-scattering data can be described using the same geometry parameters and the same energy dependence on the strength of the real potential.

To extract the Coulomb correction ΔV_c to the real central potential, the proton-scattering data of De Leo *et al.*[2,36] and de Swiniarsi *et al.*[1] were analyzed with the same nuclear model used in the present CC analysis of the neutron-scattering data. The central potential geometry parameters, the deformation parameters, and the spin-orbit potential parameters were all fixed to the values deduced in the neutron analysis. The potential strengths V_R, W_D, and W_V were searched on at each energy. The resulting fits to the data are represented by the dashed curves and are labeled as parameter set C in Figs. 16 and 17. The description of the $\sigma(\theta)$ data for elastic scattering is quite good except at the extreme backward angles where the influence of indirect reaction processes is greatest. Better fits were obtained to the inelastic $\sigma(\theta)$ data; however, at extreme back angles the trend of the calculations seemed higher than that suggested by the data. The spin-orbit parameters derived in the neutron analysis produced good representations of the $A_y(\theta)$ data for elastic scattering and reasonable fits to the inelastic

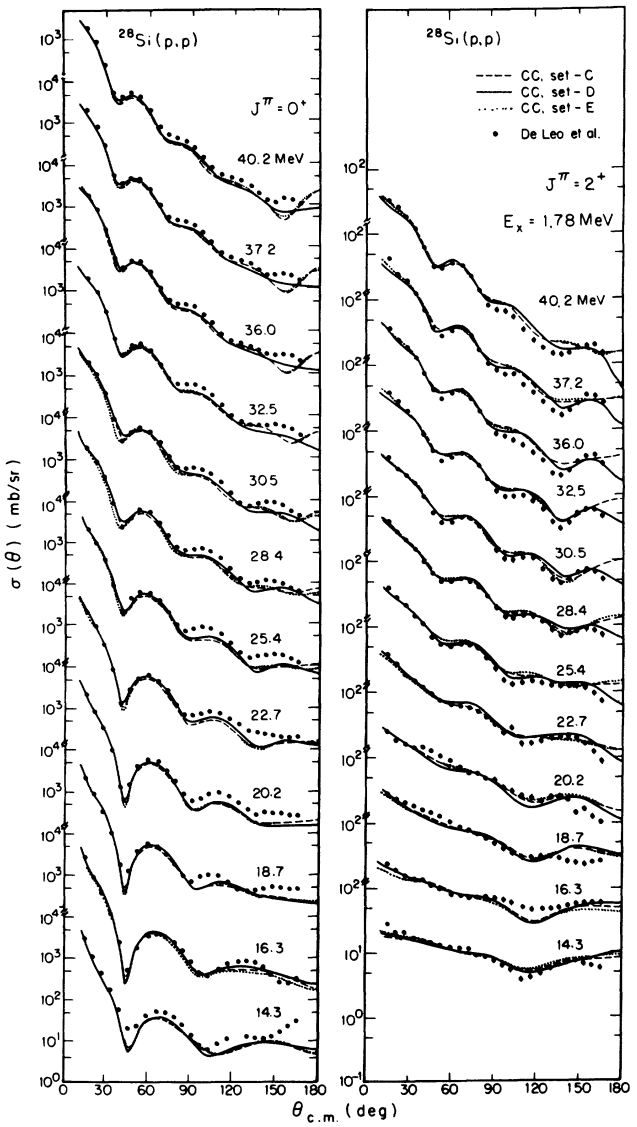

FIG. 16. Comparison of CC calculations to $\sigma(\theta)$ data for elastic and inelastic scattering of protons from ^{28}Si. The data are from Refs. 2 and 36. See text for descriptions of the curves.

scattering data, particularly above 20 MeV.

The resulting potential strengths for the real well V_R are plotted in Fig. 18 as open circles in comparison to the corresponding values obtained in the neutron analysis (solid circles). The solid and dashed lines in Fig. 18 are least-square fits to V_R for neutrons and protons, respectively. The fits were made with the constraint that the slope of the line used to describe the proton points be the same as that derived in fitting the neutron data. Assuming the slopes of the lines are correct, the uncertainties in the intercepts for the neutron and proton lines are ± 0.91 and ± 0.70 MeV, respectively. Thus, the Coulomb correction to the real potential ΔV_c is 0.33 ± 1.15 MeV. This is roughly 5.5 times smaller than the anticipated value[35] of 1.85 MeV obtained by modeling ^{28}Si as a uniform charge distribution of radius $R_c = r_c A^{1/3}$ with $r_c = 1.25$ fm.

Within the uncertainty of its determination, ΔV_c is consistent with zero. This result is similar to the previous findings of Winfield *et al.*,[4] implying that the real parts of the optical-model potential for neutron and proton scattering from ^{28}Si are indistinguishable. This suggests that some mechanism must be compensating for the known momentum shift of the incident protons. One possibility, as cited in Ref. 4, is charge symmetry breaking in the nuclear force. The best experimental values of the N-N scattering lengths are $a_{pp} = -17.900 \pm 0.005$ and $a_{nn} = -18.50 \pm 0.05$ fm,[37] which indicate a small violation of charge symmetry. According to Winfield *et al.*[4] this difference in N-N scattering lengths produces a 5% deeper potential for neutron scattering than for proton scattering from ^{28}Si. This is about the same size as the

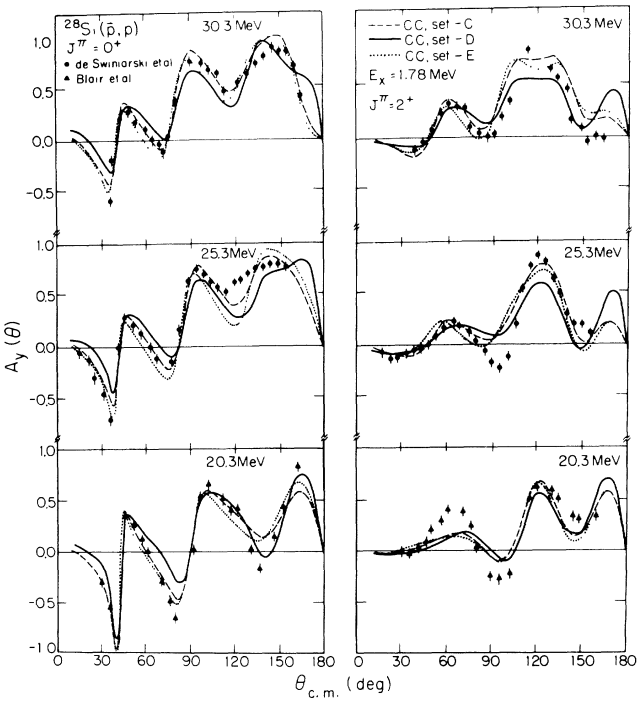

FIG. 17. Comparisons of CC calculations to $A_y(\theta)$ data for elastic and inelastic scattering of protons. The data are from Ref. 1. See text for descriptions of the curves.

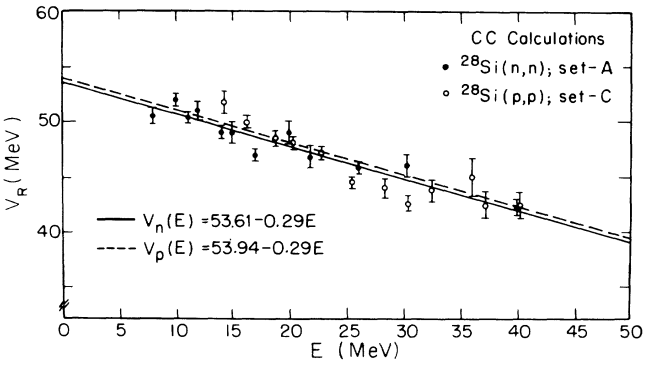

FIG. 18. Plot of potential strengths of the real well vs incident projectile energy. Comparison of (n,n) and (p,p) analyses to extract the Coulomb correction to the real part of the optical-model potential. The solid and dashed lines are least-square fits to the neutron and proton potential points, respectively.

value expected for ΔV_c based on the energy dependence of $V(E)$, but it is in the opposite direction. However, even though the CSB effects are the correct magnitude and in the proper direction to explain the small observed ΔV_c, nucleon scattering from ^{28}Si is a many-body system over which most of the fundamental N-N forces are averaged and in which detailed knowledge about the effects of the nuclear medium is critical for proper interpretation of the system. Another explanation for the small ΔV_c is simply that the influence of open reaction channels on scattering observables for the ^{28}Si$+n$ and ^{28}Si$+p$ systems is isospin dependent. For instance, the cross sections and Q values for the $(n,\text{particle})$ reactions are quite different from the corresponding $(p,\text{particle})$ reactions. Within the approximations of the CC model, these differences should be reflected in a natural way in the parametrization of the imaginary potential.

B. Coulomb correction to the imaginary potential

Because of the ambiguities between W_D and W_V, it is not very useful to make comparisons of these parameters obtained in different analyses, even if the same geometries are used. Consequently, in extracting the Coulomb correction terms to the imaginary parts of the optical potential, volume integrals per nucleon (J_W/A) are usually compared instead of potential strengths. In the upper half of Fig. 19 the horizontal band represents an energy-independent least-squares fit (and its associated uncertainty) to the values of J_W/A derived in the neutron analysis. The 8 MeV point was excluded from the fit. In fitting the neutron data the points above 25 MeV were given less weight than the lower energy points, since they appear to be systematically too high (also see Fig. 13). The weighted average of the neutron points was $(J_W/A)_n = 96.46 \pm 4.12$ MeV·fm.[3] The Coulomb correction to the imaginary potential $(\Delta J_W/A)_c$ was defined as

$$(\Delta J_W/A)_c = (J_W/A)_p - (J_W/A)_n$$
$$= (J_W/A)_p - 96.46 \text{ MeV·fm}^3 .$$

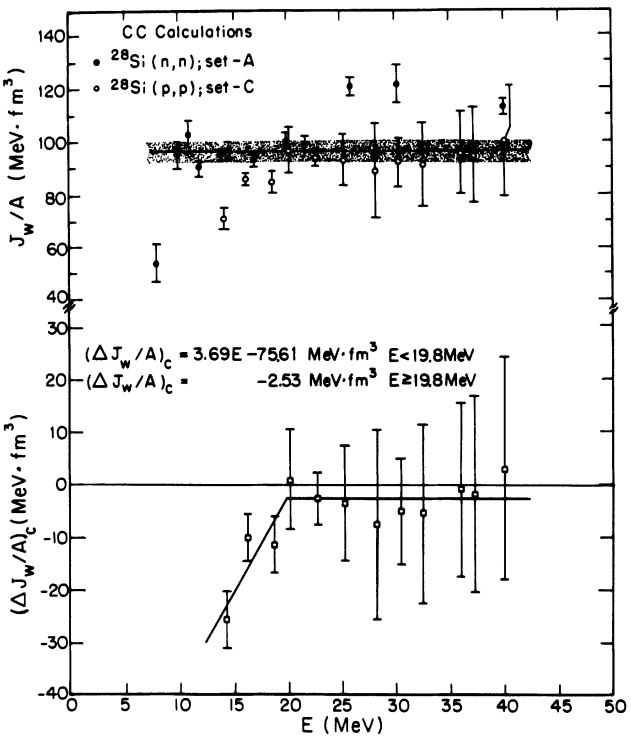

FIG. 19. Plot of volume integrals per nucleon of the imaginary potential vs incident projectile energy. Comparison of (n,n) and (p,p) analyses to extract the Coulomb correction to the imaginary part of the optical-model potential. Fits to the data points are described in the text.

The resulting volume integrals for the Coulomb correction are plotted in the lower half of Fig. 19. A least-squares fit to these $(\Delta J_W/A)_c$ points yielded

$$(\Delta J_W/A)_c=[(3.69\pm0.26)E-(75.61\pm4.36)]\ \text{MeV}\cdot\text{fm}^3$$

for $E<19.8$ MeV,

and

$$(\Delta J_W/A)_c=[-(2.53\pm3.25)]\ \text{MeV}\cdot\text{fm}^3$$

for $E\geq 19.8$ MeV.

The values obtained in this analysis for neutron energies below 20 MeV are very similar to those deduced by DeVito *et al.*[4] in their SOM analysis. However, the present results are considerably smaller than those of DeVito *et al.*[4] for neutron energies above 20 MeV. These differences are probably due to coupling effects, as mentioned by Winfield *et al.*,[4] and to our ignoring the uncharacteristically high values of W_D at 26 and 30 MeV for the neutron case.

C. Sensitivity of fits to optical-model parameters for ^{28}Si(p,p)

To investigate the poor fits to the backward angle $\sigma(\theta)$ data for proton elastic scattering, the geometry parameters were searched on individually. The back angle $\sigma(\theta)$ was most sensitive to r_R and a_{so}. Decreasing r_R and/or increasing a_{so} improved the description of the back angle $\sigma(\theta)$ data but slightly degraded the quality of the fits to the $A_y(\theta)$ data for elastic scattering. To improve the fits to the proton data the spin-orbit parameters used in parameter set *C*, which were the same as those used in our neutron analysis, were replaced by the parameters of De Leo *et al.*[2] ($V_{so}=6.0$ MeV, $r_{so}=1.07$ fm, $a_{so}=0.78$ fm, and $\delta_{so}=\delta_c$). For direct comparison between the potential strengths obtained in this analysis with those derived in set *C*, the geometry parameters and the deformation parameters of the central potential were fixed to the values used in set *C*. The fits were optimized at each energy by searching on V_R, W_D, and W_V. The calculated $\sigma(\theta)$ and $A_y(\theta)$ are displayed as solid curves in Figs. 16 and 17, and the resulting parameters are referred to as set *D*. The descriptions of the backward angle $\sigma(\theta)$ data were improved, but only slightly, while the fits to the $A_y(\theta)$ data for elastic scattering were somewhat worsened. The description of the $A_y(\theta)$ data for inelastic scattering was roughly the same as that obtained with parameter set *C*. The resulting potential strengths were statistically indistinguishable from those in set *C*. This is an indication that our technique for extracting the Coulomb correction to the proton potential is only weakly dependent on the choice of parameters for the spin-orbit potential, provided the parameters produce reasonable fits to the data.

D. Test for CSB and isospin dependent effects in ^{28}Si(n,n) and ^{28}Si(p,p) scattering

We further extended the comparisons of ^{28}Si(n,n) and ^{28}Si(p,p) to better understand the differences in the interaction of protons and neutrons with this $T=0$ nucleus and to try to disentangle the nuclear force effects from the pure Coulomb influences in the scattering process. The proton data were reanalyzed, and this time the momentum shift of the incident protons due to the Coulomb repulsion by the charge in the target nucleus was explicitly incorporated in the CC calculations. The V_R's for the new analysis were derived from the parametrization of the real potential strengths in set *B* of the neutron analysis. The values of V_R were computed by shifting the neutron values down in energy an amount ΔE_c, the mean energy shift of the incident protons. That is, $V_p(E)=V_n(E-\Delta E_c)$. The value of $\Delta E_c=5.7$ MeV, which was deduced by Winfield *et al.*[4] and corresponds to a ΔV_c of 1.65 MeV for the central potential, was used in these calculations. All geometry parameters and deformations parameters were fixed to the values used in the neutron analysis. The spin-orbit potential parameters were also held to the values derived in the neutron analysis. Single-energy fits were performed by searching on W_D and W_V. The resulting fits are shown in Figs. 16 and 17 as the dotted curves and are referred to as set *E*. These calculations illustrate that equal quality fits to the proton data can be achieved either by searching on V_R, W_D, and W_V as in set *C* or by starting with the V_R from the neutron analysis and applying the proper Coulomb correction to it (without including the canceling effect due to CSB) and then searching only on W_D and W_V. The ΔV_c deduced in the above two approaches were 0.33

and 1.65 MeV, respectively. The difference in the value of ΔV_c is mainly due to ambiguities between the real and imaginary parts of the optical-model potential. This ambiguity in trading off the effects of the Coulomb interaction between the real and imaginary potentials causes at least a 1.3 MeV uncertainty in determining ΔV_c. Such a large uncertainty suggests that the uncertainty assigned by Winfield *et al.*[4] to their determination of the CSB term in the ^{28}Si+nucleon scattering system should be increased. These large errors indicate that the extraction of CSB effects from many-body systems such as ^{28}Si+nucleon is an extremely complicated task, which is very model dependent and somewhat limited by the accuracy of nucleon-nucleus scattering data.

Figure 20 shows the resulting J_W/A from the above calculations plotted as a function of $E_p - \Delta E_c$ in comparison with the values obtained in the neutron analysis. Such a comparison should reflect isospin dependences in the ^{28}Si+nucleon interaction. The neutron and proton parameters are statistically indistinguishable, except around 30 MeV. This difference is primarily caused by the abnormally large increase in the volume integrals of the neutron analysis between 22 and 26 MeV, suggesting the opening of a strong(n,particle) channel or the excitation of a broad resonance, neither of which is anticipated. No such broad structure is evident in the proton parameters in Fig. 20. More neutron-scattering data in the energy range from 22 to 50 MeV would be helpful for understanding this anomalous behavior. High accuracy measurements of the $\sigma(\theta)$ for elastic scattering, especially in the backward angle region, and for inelastic scattering to the 2^+ and 4^+ states would be extremely useful, since the calculations of these observables are quite sensitive to W_D as illustrated in Fig. 11 by comparing the solid and dashed curves.

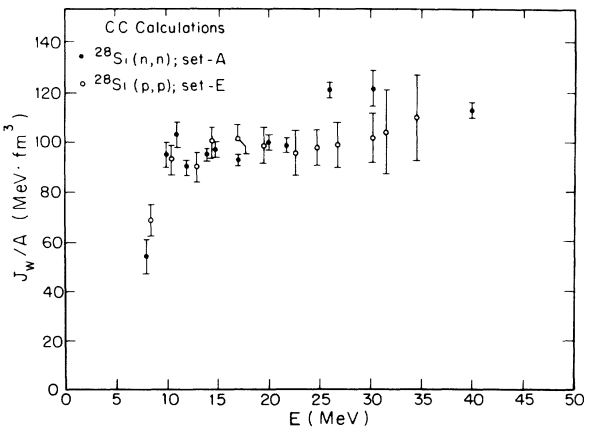

FIG. 20. Comparison of volume integrals per nucleon for the imaginary part of the optical-model potential for neutron and proton scattering. The proton points have been shifted down in energy by $\Delta E_c = 5.7$ MeV to account for the momentum loss of the incident protons due to Coulomb repulsion by the target nucleus.

IX. SUMMARY AND CONCLUSIONS

The most complete set of differential cross sections and analyzing powers for neutron scattering from ^{28}Si over the 8–40 MeV energy range has been compiled and described within the framework of a symmetric rotational model. Compound nucleus contributions to the data for elastic scattering and inelastic scattering to the 2^+ state were found to be negligible above 14 MeV. This was not the case for inelastic scattering to the 4^+ state, in which compound nucleus effects were significant up to about 20 MeV.

Sensitivities of the observables to the magnitude and signs of the deformation parameters were studied. The spin-orbit potential was found to be about 20% more deformed than the central potential; that is, $\delta_{so} = (1.2 \pm 0.2)\delta_c$. Better fits to the back angle $\sigma(\theta)$ data for elastic scattering were obtained with an oblate-shaped potential ($\beta_2 < 0$). The $\sigma(\theta)$ for inelastic scattering to the 2^+ state required a positive β_4. In addition, the back angle $A_y(\theta)$ for inelastic scattering to the 2^+ and 4^+ states were extremely sensitive to the signs of β_2 and β_4, with the data preferring $\beta_2 < 0$ and $\beta_4 > 0$. These findings are consistent with the theoretical predictions in Refs. 25 and 31. The values of $\beta_2 = -0.38 \pm 0.01$ and $\beta_4 = +0.18 \pm 0.02$ deduced in the present work are consistent with the results of other (n,n') and (p,p') scattering measurements.[1–3]

The values for the intrinsic quadrupole moment Q_0 deduced in the present analysis of ^{28}Si(n,n') data and other hadron-scattering experiments[1–3] are consistently larger than the values extracted for this quantity from (e,e') and EM studies.[27–30] Although the differences are relatively small, generally less than two to three standard deviations, this feature could be evidence for: (i) density-dependent effects, (ii) breakdown of the collective model, or (iii) subtle differences between the charge and matter distributions in ^{28}Si. According to Satchler's theorem,[34] the normalized nuclear moments of a deformed optical potential equal the moments of the nuclear matter distribution only if the optical potential can be derived from a density-independent folding potential. Density dependence in the effective N-N interaction used in a folding model tends to enhance the size of the quadrupole moment.[26] The direction of this effect is consistent with the discrepancies between hadron-scattering experiments and (e,e') and EM measurements. A failure of the collective model to properly describe the nuclear motion should not cause the above discrepancies, since the hadron-scattering, (e,e') and EM data were all analyzed with the same type of collective model.[26,38] Furthermore, it has been demonstrated that the proton and neutron distributions in light nuclei are approximately equal. Therefore, in the case of light nuclei like ^{28}Si, it is reasonable to conclude that the enhanced Q_0 deduced in the present analysis and in other hadron-scattering experiments is more likely to be caused by a density dependence in the effective N-N interaction needed to generate the optical potential than by a difference in the charge and matter distributions.

The models used to extract the hexadecapole moment H_0 are extremely sensitive to: (i) the effects caused by

density dependence in the effective N-N interaction used in the folding model, (ii) breakdown of the collective nuclear model, and (iii) subtle differences between the charge and matter distributions. It is probably reasonable to assume that the symmetric rotational model is capable of determining H_0 to $\pm 5\%$. Therefore, the large discrepancy between the value for H_0 obtained in the present work and that from (e,e') measurements must be caused by the combination of density dependence in the effective N-N interaction and small differences in the charge and matter distributions. Our results suggest that the neutron distribution is slightly more deformed than the protons.

The standard Coulomb correction terms to the real and imaginary parts of the optical-model potential have been determined. The Coulomb correction to the real well was found to be very small, that is, $\Delta V_c = 0.33 \pm 1.15$ MeV. This is roughly five times smaller than the anticipated value of 1.8 MeV obtained when ^{28}Si is modeled as a uniformly charged sphere. The corrections to the imaginary potential were also small, provided the uncharacteristic behavior of the neutron parameters above 20 MeV is neglected. Better neutron data in the 25–50 MeV energy region is desirable to clarify this behavior.

To better understand the small values for the Coulomb correction terms extracted using the standard method and to address the issue of charge symmetry breaking effects in the ^{28}Si+nucleon scattering system, the ^{28}Si(p,p) data were reanalyzed using the geometry parameters of our ^{28}Si(n,n) analysis. The potential strengths of the real well were computed from the neutron values by reducing the (proton) projectile energy by an amount $\Delta E_c = 5.70$ MeV derived by Winfield *et al.*,[4] thus giving $V_p(E) = V_n(E - \Delta E_c)$. The surface and volume imaginary potential strengths were left as free parameters in single-energy searches. The volume integrals of the imaginary potentials for the neutron and proton analyses were compared by shifting the incident proton energy down by ΔE_c. It was found that when the proton energy is adjusted for the momentum shift due to the Coulomb repulsion of the target nucleus, the volume integrals of the real and imaginary potentials for proton and neutron scattering from ^{28}Si are indistinguishable within the assigned uncertainties. This latter approach for comparing ^{28}Si(n,n) and ^{28}Si(p,p) scattering processes strongly suggests that [within the framework of this analysis and the accuracy of the available (n,n) and (p,p) data] the observable differences between neutron and proton scattering from ^{28}Si can be accounted for without introducing charge symmetry breaking. In fact, our calculations show that the primary difference between the neutron- and proton-scattering potentials can be solely attributed to the Coulomb force. Although the influences of CSB are undoubtedly present in nucleon-nucleus scattering, the extraction of these effects from many-body systems is an enormously complex problem which is extremely model dependent and somewhat limited by the accuracy of nucleon-nucleus scattering data.

This work was supported by the U.S. Department of Energy, Office of High Energy and Nuclear Physics, under Contract No. DE-AC05-76ER01067.

---

*Present address: Physics Department, Ohio University, Athens, OH 45701.

†Present address: Radiology Department, Duke University Medical Center, Durham, NC 27706.

‡Present address: Indiana University Cyclotron Facility, Bloomington, IN 47405.

§Permanent address: Los Alamos National Laboratory, Physics Division, Los Alamos, NM 87545.

**Permanent address: Department of Physics, University of Birmingham, Birmingham, U.K.

[1]R. de Swiniarski and D. L. Pham, Lett. Al Nuovo Cimento **16**, 391 (1976); R. de Swiniarski, F. G. Resmini, D. L. Hendrie, and A. D. Bacher, Nucl. Phys. **A261**, 111 (1976); R. de Swiniarski, H. E. Conzett, C. R. Lamontagne, B. Frois, and R. J. Slobodrian, Can. J. Phys. **51**, 1293 (1973); A. G. Blair, C. Glashausser, R. de Swiniarski, J. Goudergues, R. Lombard, B. Mayer, J. Thirion, and P. Vaganov, Phys. Rev. C **1**, 444 (1970).

[2]R. De Leo, G. D'Erasmo, A. Pantaleo, G. Pasquariello, G. Viesti, M. Pignanelli, and H. V. Geramb, Phys. Rev. C **19**, 646 (1979).

[3]R. Alarcon and J. Rapaport, Nucl. Phys. **A458**, 502 (1986); (private communication); J. Böttcher, H. Blank, E. Finckh, C. Forstner, W. Jaumann, G. Schall, H. Scheuring, U. Schneidereit, K. Stauber, A. Weipert, W. Tornow, and E. Woye, J. Phys. G **9**, L65 (1983); (private communication); R. C. Tailor, Ph.D. dissertation, Ohio University, 1982; S. Kliczewski and Z. Lewandowski, Nucl. Phys. **A304**, 269 (1978); A. W. Obst and J. L. Weil, Phys. Rev. C **7**, 1076 (1972); G. Haouat, Ch. Lagrange, R. de Swiniarski, F. Dietrich, J. P. Delaroche, and Y. Patin, *ibid.* **30**, 1795 (1984); (private communication).

[4]R. P. DeVito, S. M. Austin, U. E. P. Berg, R. De Leo, and W. A. Sterrenburg, Phys. Rev. C **28**, 2530 (1983); (private communication); J. S. Winfield, S. M. Austin, R. P. DeVito, U. E. P. Berg, Ziping Chen, and W. Sterrenburg, Phys. Rev. C **33**, 1 (1986).

[5]Ph. Martin, Nucl. Phys. **A466**, 119 (1987).

[6]C. R. Howell, in *Neutron-Nucleus Collisions—A Probe of Nuclear Structure (Burr Oak State Park, Glouster, Ohio)*, Proceedings of the Conference on Neutron-Nucleus Collisions—A Probe of Nuclear Structure, AIP Conf. Proc. No. 124, edited by J. Rapaport, R. W. Finlay, S. M. Grimes, and F. S. Dietrich (AIP, New York, 1984).

[7]ENDF/B–5 data files for ^{28}Si, National Nuclear Data Center, Brookhaven National Laboratory (1979); D. C. Larson, D. M. Hetrick, and J. A. Harvey, Bull. Am. Phys. Soc. **25**, 543 (1980); (private communication).

[8]C. R. Howell and R. L. Walter, IEEE Trans. Nucl. Sci. **NS-30**, 1132 (1983).

[9]G. M. Honoré, W. Tornow, C. R. Howell, R. S. Pedroni, R. C. Byrd, and R. L. Walter, Phys. Rev. C **33**, 1129 (1986); W. Tornow, E. Woye, G. Mack, C. E. Floyd, K. Murphy, P. P. Guss, S. A. Wender, R. C. Byrd, R. L. Walter, T. B. Clegg,

and H. Leeb, Nucl. Phys. **A385**, 373 (1982).
[10]S. A. Wender, C. E. Floyd, T. B. Clegg, and W. R. Wylie, Nucl. Instrum. Methods **174**, 341 (1980); S. A. Wender, IEEE Trans. Nucl. Sci. **NS-28**, 1465 (1981).
[11]G. G. Ohlsen and P. W. Keaton, Jr., Nucl. Instrum. Methods **109**, 41 (1973).
[12]W. Tornow, E. Woye, G. Mack, C. E. Floyd, K. Murphy, P. P. Guss, S. A. Wender, R. C. Byrd, R. L. Walter, and T. B. Clegg, Nucl. Phys. **A385**, 373 (1982).
[13]F. M. Mann, Hanford Engineering Development Laboratory Report HEDL-TME 78-83 UC-79d, 1979.
[14]A. Gilbert and A. G. W. Cameron, Can. J. Phys. **43**, 1446 (1965).
[15]J. Raynal, computer code ECIS79 (unpublished); International Atomic Energy Agency Report No. SMR-918, 281, 1972.
[16]F. G. Perey, Phys. Rev. **131**, 745 (1963).
[17]C. M. Perey and F. G. Perey, Phys. Rev. **132**, 755 (1963).
[18]H. H. Duhm, Nucl. Phys. **A118**, 563 (1968).
[19]B. Mainsbridge, T. W. Bonner, and T. A. Rabson, Nucl. Phys. **48**, 83 (1963).
[20]S. M. Grimes, Nucl. Phys. **A124**, 369 (1969).
[21]D. W. Mingay, J. P. J. Sellschop, and P. M. Johnson, Nucl. Instrum. Methods **94**, 497 (1971).
[22]H. Gruppelaar and G. Reffo, Nucl. Science Eng. **62**, 62 (1977).
[23]C. E. Floyd, R. L. Walter, and R. G. Seyler, Bull Am. Phys. Soc. **27**, 722 (1982).
[24]W. T. H. Van Oers, Huang Haw, N. E. Davison, A. Ingemarsson, B. Fagerstrom, and G. Tibell, Phys. Rev. C **10**, 307 (1974).
[25]H. C. Lee and R. Y. Cusson, Ann. Phys. **72**, 353 (1972).
[26]R. S. Mackintosh, Nucl. Phys. **A266**, 379 (1976).
[27]Y. Horikawa, Y. Torizuka, A. Nakada, S. Mitsunobu, Y. Kojima, and M. Kimura, Phys. Lett. **36B**, 9 (1971).
[28]Yataro Horikawa, Prog. Theor. Phys. **47**, 867 (1972).
[29]G. C. Ball, O. Häusser, T. K. Alexander, W. G. Davies, J. S. Forster, I. V. Mitchell, J. R. Breene, and D. Horn, Nucl. Phys. **A349**, 271 (1980).
[30]J. S. Forster, T. K. Alexander, G. C. Ball, W. G. Davies, I. V. Mitchell, and K. B. Winterbon, Nucl. Phys. **A313**, 397 (1979).
[31]H. R. Jaqaman and L. Zamick, Phys. Rev. C **30**, 1719 (1984).
[32]A. Bohr and B. Mottelson, *Nuclear Structure* (Benjamin, New York, 1969), Vol. II, p. 44.
[33]P. H. Stelson and L. Grodzins, Nucl. Data Sheets **1**, 21 (1965).
[34]G. R. Satchler, J. Math. Phys. **13**, 1118 (1972).
[35]G. R. Satchler, in *Isospin in Nuclear Physics,* edited by D. H. Wilkinson (North-Holland, Amsterdam, 1969); J. Rapaport, J. D. Carlson, D. Bainum, T. S. Cheema, and R. W. Finlay, Nucl. Phys. **A286**, 232 (1977).
[36]R. De Leo, G. D'Erasmo, E. Fabrici, S. Micheletti, A. Pantaleo, M. Pignanelli, and F. G. Resmini, Instituto Nazionale di Fisica Nucleare, Sezione di Milano, Report No. INFN/BE-78/8, 1978.
[37]O. Dumbrajs, R. Koch, H. Pilkuhn, G. C. Oades, H. Behrens, J. J. DeSwart, and P. Kroll, Nucl. Phys. **B216**, 277 (1983).
[38]R. S. Mackintosh and L. J. Tassie, Nucl. Phys. **A222**, 187 (1974).

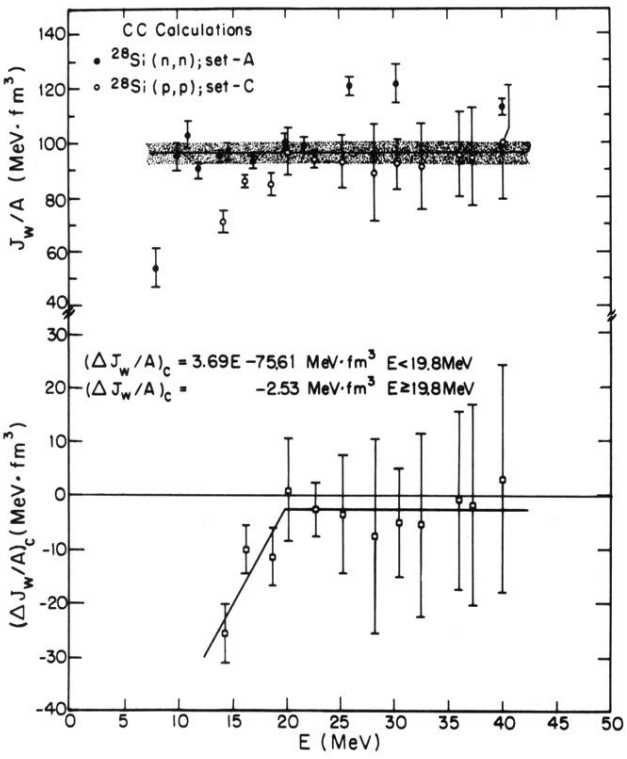

FIG. 19. Plot of volume integrals per nucleon of the imaginary potential vs incident projectile energy. Comparison of (n,n) and (p,p) analyses to extract the Coulomb correction to the imaginary part of the optical-model potential. Fits to the data points are described in the text.